Specific Targeting of Mesothelin-Expressing Malignant Cells Using Nanobody-Functionalized Magneto-Fluorescent Nanoassemblies

Tina Briolay, Judith Fresquet, Damien Meyer, Brigitte Kerfelec, Patrick Chames, Eléna Ishow, Christophe Blanquart

International Journal of Nanomedicine

Dovepress
open access to scientific and medical research

Open Access Full Text Article

ORIGINAL RESEARCH

Specific Targeting of Mesothelin-Expressing Malignant Cells Using Nanobody-Functionalized Magneto-Fluorescent Nanoassemblies

Tina Briolay[1], Judith Fresquet[1], Damien Meyer[2], Brigitte Kerfelec[2], Patrick Chames[2], Eléna Ishow[3], Christophe Blanquart[1]

[1]Nantes Université, INSERM UMR 1307, CNRS UMR 6075, Université d'Angers, CRCI2NA, Nantes, F-44000, France; [2]Aix Marseille Univ, CNRS, INSERM, Institut Paoli-Calmettes, CRCM, Marseille, France; [3]Nantes Université, CNRS, CEISAM, UMR 6230, Nantes, F-44000, France

Correspondence: Christophe Blanquart, CRCI2NA, INSERM UMR 1307/CNRS UMR 6075, IRS-UN, 8 Quai Moncousu, BP70721, Cedex 1, Nantes, 44007, France, Tel +33 228 080 238, Email christophe.blanquart@inserm.fr

Introduction: Most current anti-cancer therapies are associated with major side effects due to a lack of tumor specificity. Appropriate vectorization of drugs using engineered nanovectors is known to increase local concentration of therapeutic molecules in tumors while minimizing their side effects. Mesothelin (MSLN) is a well-known tumor associated antigen overexpressed in many malignancies, in particular in malignant pleural mesothelioma (MPM), and various MSLN-targeting anticancer therapies are currently evaluated in preclinical and clinical assays. In this study, we described, for the first time, the functionalization of fluorescent organic nanoassemblies (NA) with a nanobody (Nb) targeting MSLN for the specific targeting of MSLN expressing MPM cancer cells.

Methods: Cell lines from different cancer origin expressing or not MSLN were used. An Nb directed against MSLN was coupled to fluorescent NA using click chemistry. A panel of endocytosis inhibitors was used to study targeted NA internalization by cells. Cancer cells were grown in 2D or 3D and under a flow to evaluate the specificity of the targeted NA. Binding and internalization of the targeted NA were studied using flow cytometry, confocal microscopy and transmission electron microscopy.

Results: We show that the targeted NA specifically bind to MSLN-expressing tumor cells. Moreover, such functionalized NA appear to be internalized more rapidly and in significantly larger proportions compared to naked ones in MSLN+ MPM cells, thereby demonstrating both the functionality and interest of the active targeting strategy. We demonstrated that targeted NA are mainly internalized through a clathrin-independent/dynamin-dependent endocytosis pathway and are directed to lysosomes for degradation. A 3D cell culture model based on MSLN-expressing multicellular tumor spheroids reveals NA penetration in the first superficial layers.

Conclusion: Altogether, these results open the path to novel anticancer strategies based on MSLN-activated internalization of NA incorporating drugs to promote specific accumulation of active treatments in tumors.

Keywords: mesothelin, targeting, nanoassemblies, nanobody, cancer

Introduction

Malignant pleural mesothelioma (MPM) is an aggressive cancer of the pleura that usually develops 3 to 4 decades following exposure to asbestos. It is a relatively rare disease that is typically associated with a poor prognosis, being responsible for approximately 30,000 annual deaths worldwide (https://gco.iarc.fr/today/data/factsheets/cancers/18-Mesothelioma-fact-sheet.pdf). For years, the first-line treatment of MPM has consisted of systemic chemotherapy regimens including a platinum-derivate (either cisplatin or carboplatin) and an antimetabolite (pemetrexed), but the outcomes remain unsatisfactory.[1,2] New therapeutic alternatives are currently being tested in clinical trials, such as immune checkpoint inhibitors[3] and targeted therapies.[4] The recent approval of nivolumab (anti-PD-1) plus ipilimumab (anti-CTLA-4) as first-line treatment of advanced unresectable mesothelioma, the first Food and Drug Administration (FDA) approval since pemetrexed and cisplatin, represents a major progress in MPM management.[4,5] However, the median overall survival of patients, despite treatment with this protocol, remains low (around 18 months). There is therefore an urgent need for new therapeutic alternatives to treat MPM patients.

Received: 14 September 2023
Accepted: 14 December 2023
Published: 20 January 2024

The efficiency of anti-cancer therapies and the development of new molecules are usually limited by systemic toxicity and solubility concerns. To overcome these problems, strategies of vectorization have been developed to increase circulation time of active molecules in blood, reduce their toxicity and increase their accumulation in tumors.[6] This approach was notably evaluated in MPM using an untargeted liposomal doxorubicin.[7,8] The efficiency of this strategy was however limited by the still insufficient accumulation of the active molecule in the tumors.[7,8] Active targeting of nanovectors to tumors, mostly thanks to antibody fragments, has been described to promote active uptake of the nanovectors by tumor cells. It also enables retention and enrichment of the nanovectors in tumors expressing the target when compared to untargeted nanovectors.[6] Recent data, obtained in mice with doxorubicin liposomes endowed with a CD44 targeting ability, showed higher uptake of doxorubicin into MPM tumors and a better clinical response.[9] However, an active targeting strategy requires the identification of a relevant tumor associated antigen (TAA) to obtain a highly specific delivery of therapies to tumor cells.

Mesothelin (MSLN) is a TAA normally restricted to mesothelial tissues of the body but overexpressed in a broad range of solid tumors.[10–12] For this reason, MSLN has been considered a promising target for the development of targeted therapies against various cancers.[10,13] Several MSLN-targeted therapies have been developed including antibody-drug conjugates, radio-immunoconjugates, T cell engagers, immunotoxins, and adoptive cellular therapies.[1,4,14,15] However, only few studies depict nanovectors targeted to MSLN[16–19] for drug delivery, while the targeting of other TAA is widely documented.[20,21] A large number of Phase II clinical trials testing MSLN-targeted therapies in MPM were reported and demonstrated the safety of the approach.[13] Even if the contribution of MSLN-targeted therapies on overall patients' survival still has to be demonstrated in MPM, such strategies have proven interesting in other MSLN expressing cancers such as ovarian carcinoma.[22,23] Targeting this TAA thus remains of interest for cancer-targeted therapy.

In this study, we developed magneto-fluorescent organic nanoassemblies (FONmag) actively targeted to MSLN. Previously described FONmag[24] were functionalized with an anti-MSLN nanobody[25] by copper-free click chemistry. After physico-chemical characterization of functionalized nanoassemblies (NA), their internalization by cancer cells was studied taking advantage of the multimodal imaging properties of the NA using flow cytometry, confocal microscopy and transmission electron microscopy. Specificity of functionalized NA was evaluated by confocal microscopy in 2 or 3D culture models, the latter used to mimic some of the in vivo constraints of tumors. Finally, experiments under a flow of culture medium were performed to mimic hydrodynamic constraints associated with the intrapleural injection of therapies in the context of MPM.

Materials and Methods

Nanoassemblies (NA) Synthesis

All reagents, chemicals and solvents were purchased from Merck (Sigma-Aldrich).

FONmag Preparation

FONmag magneto-fluorescent nanoassemblies were prepared following a similar protocol reported in literature.[26] A solution of fluorescent phosphonic compound[27] dissolved in tetrahydrofuran (50 µL, 0.1 wt. %) was added under vigorous stirring to a solution of maghemite nanoparticles in nitric acid (2.5 mL, 0.006 wt. %, pH = 1.2). Polyacrylic acid (2.1 kDa, 5 mg) was added as powder; ammonium hydroxide (1 $mol.L^{-1}$) was added dropwise under stirring until pH 9 was reached. The resulting translucent solution was allowed to stir for a further 30 min and dialyzed using a Spectra Por membrane (Standard Grade Regenerated Cellulose; cut-off: 8–10 kD; Dutscher – 059011) against Millipore water (600 mL) over 24 h and concentrated 6 times using Vivaspin® (Sartorius) dialysis tubes (MWCO 100 kDa – VS0641).

PolyEthylene Glycol (PEG) Carboxylic Linker

The PEG carboxylic acid linker was synthesized following a previously described procedure.[27] Briefly, poly(ethylene glycol) bis(3-aminopropyl) terminated polymer (200 mg, 0.13 mmol) (M_W ~1 500 $g.mol^{-1}$) was dissolved in acetonitrile (5 mL). A solution of succinic anhydride (13 mg, 0.13 mmol) dissolved in acetonitrile (5 mL) was added dropwise to the polymer solution. The reaction mixture was left at room temperature under stirring for 12 h. After solvent removal under vacuum, a yellowish wax formed over time (quant.). ^{1}H NMR (300 MHz, D_2O) δ: 3.78 (120 H, m), 3.63 (2 H, t, $^3J(H, H) = 3$ Hz), 3.34 (2 H, t, $^3J(H, H) = 6$ Hz), 2.64 (2 H, t, $^3J(H, H) = 5$ Hz), 2.58 (2 H, t, $^3J(H, H) = 6$ Hz), 1.87 (2 H, qt, $^3J(H, H) = 6$ Hz) ppm. FTIR (ATR) σ: 2881 (C-H), 2861 (C-H), 1726 (C=O(-O)), 1648 (C(=O)-N, 1341 (C(=O)-O), 1102 (C-O) cm^{-1}.

Coupling FONmag Surface with a PEG Linker

1-ethyl-3-(3-dimethylaminopropyl) carbodiimide (EDC) and N-hydroxysulfosuccinimide sodium salt (sulfo-NHS) solutions (50 mmol.L^{-1}) were prepared using 2-morpholinoethanesulphonic acid (MES) buffer solution (0.1 mol.L^{-1}). Equimolar amounts of EDC and sulfo-NHS solutions (200 µL each) were added to each aliquot of concentrated FONmag solution previously diluted by half (total volume 2 mL). The dispersions were stirred using a rotating wheel for 10 min. The formed precipitate was redissolved by adding a few drops of saturated $NaHCO_3$ until pH 7 was reached. Aliquots (400 µL) of an aqueous solution of the PEG linker (50 mmol.L^{-1}) were added to each vial of activated-FONmag, and the vials were stirred overnight. Dialysis using Spectra Por membrane (Standard Grade Regenerated Cellulose; cut-off: 8–10 kD; Dutscher – 059011) against Millipore water (MWCO 6–8 kDa) was performed over two days.

Introduction of a Clickable Agent

Final coupling with dibenzocyclooctyne-amine (DBCO) was performed following the same activation process as described above. After activation with EDC and sulfo-NHS and pH neutralization, aliquots (100 µL) of a solution of DBCO in dimethylsulfoxide (15 mmol.L^{-1}) were added to each vial and the resulting vials were stirred for one more day. Dialysis using Spectra Por membrane (Standard Grade Regenerated Cellulose; cut-off: 8–10 kD; Dutscher – 059011) (MWCO 6–8 kDa) was again performed for two days at room temperature. The resulting NA will be named FONmagc in this article.

Nanoassembly Structural and Photophysical Characterizations

Size Measurements using Dynamic Light Scattering (DLS)

Dynamic light scattering measurements were carried out at 25 °C by means of the Vasco 3 size analyzer (Cordouan Technologies, Pessac, France), equipped with a 40 mW laser diode operating at 658 nm. All data were collected in a backscattering mode at an angle of 135°. For each sample, intensity measurements were carried out in a multi-acquisition mode implying automatically adjusted correlograms and averaged measurements on six acquisitions. Z-averaged hydrodynamic diameter (D_Z) and polydispersity index (PDI) were obtained by fitting each correlogram with a cumulant-based algorithm provided by Cordouan Technologies.

Size Measurements using Transmission Electron Microscopy (TEM)

TEM analyses were performed using a MO-Jeol 1230 operated at 80 kV. All nanoassembly solutions were deposited onto holey carbon-coated copper grids (300 mesh). The mean diameter (D_{TEM}) and standard deviation (σ) were assessed by fitting with a lognormal distribution the histograms issued from counting 200 nano-objects using the free ImageJ software.

Zeta Surface Potential

Measurements of surface potential ζ were carried out by means of a Zetasizer Nano ZS ZEN 3600 (Malvern, Orsay, France). The samples were placed in disposable folded capillary cells (DTS1070). Three measurements were performed for each sample, and the zeta potential was calculated from electrophoretic mobility dispersion fitted by the Smoluchowski model.

Steady-State Photophysical Properties

UV−visible absorption spectra were recorded using a Cary 5000 spectrophotometer (Agilent, Les Ulis, France). Steady-state emission spectra were recorded using a Fluorolog 3 spectrofluorometer (Horiba, Longjumeau, France). Correction for the emission spectra with regard to the spectral response of the detector was automatically applied. Fluorescence quantum yields were determined in solution, referred to coumarin 540A in ethanol (Φ_f = 0.38).

Time-Resolved Fluorescence Measurements

Fluorescence time decays were measured in water using the fully automated spectrofluorometer (model Fluotime 300, PicoQuant) following the time-correlated single-photon counting method. Excitation was performed using a pulsed laser diode (LDH-D-C-450B) working at 450 ± 10 nm (70 ps fwhm time resolution). Fluorescence decays were recorded using a Hybrid-PMT detector combined with an acquisition temporal resolution up to 25 ps. Time fluorescence decay modeling was performed with EasyTau software.

Assessment of NA Concentration (qNano)

Single-particle tracking was performed by Tunable Resistive Pulse Sensing (TRPS) using a qNano gold device (IZON, Lyon, France). Diameter and concentration of the NA were determined using a np100 nanopore (detected range 50 −330 nm), with a 46 mm stretch and a 0.80 V voltage to obtain a 120 nA baseline (Supplementary Figure 1A and B).

Cell Culture

Malignant Pleural Mesothelioma (Meso34 and Meso13) and lung adenocarcinoma (ADCA153) cell lines were established from pleural effusions of patients in our laboratory.[28] These cell lines belong to a validated biocollection (Ministère de l'Enseignement Supérieur et de la Recherche n° DC-2011-1399 and Commission Nationale de l'Informatique et des Libertés (CNIL) n°: 1657097). Study was approved by local ethical committee, Comité de Protection des Personnes (CPP) Ouest-IV-Nantes (an independent organ from French ministry of health) (n°: 150/2007). These cells were characterized for their mutational status using targeted sequencing.[29] The stable Meso34-MSLN cell line was obtained by transduction of Meso34 cells with a human MSLN encoding lentivirus (Gift from Adusumilli PS lab, MSK, New-York, USA). MSLN overexpressing Meso34 cells were then sorted by flow cytometry after staining with a Phyco-erythryin (PE) conjugated anti-human MSLN antibody (R&D Systems FAB32652P) and amplified for the experiments. Meso34-MSLN cells were further transduced with other lentiviruses to enable stable expression of green or blue fluorescent proteins (GFP or BFP) for the coculture experiments. The A1847 ovarian carcinoma cell line was provided by P. Chames team (CRCM, Marseille, France). All cell lines were maintained in RPMI-1640 medium (Gibco) supplemented with 2 mM L-glutamine, 100 IU/mL penicillin, 0.1 mg/mL streptomycin, 10% heat-inactivated fetal calf serum (Gibco) and cultivated at 37°C in a 5% CO_2 atmosphere.

Production of the Nanobody

Anti-MSLN nanobody A1[25] (1 mg/mL in PBS) was incubated for 4 h at room temperature under shaking (400 rpm) with a 20-fold-molar excess of Azido-PEG3-Amine (Click Chemistry tools AZ101) and 20 µL of microbial transglutaminase (MTG) (Zedira E021). The reaction was stopped by addition of 40 µL of MTG blocker (Zedira C102) for 30 min at room temperature under shaking. The excess of Azido-PEG3-Amine was removed on a PD-10 desalting column. Azide functionalization of the nanobody was assessed by the coupling of 2 µg of the reaction with a 5-fold molar excess of BCN-biotin for 2 h at room temperature. Binding properties of azide-Nb A1 were evaluated by flow cytometry on MSLN-transfected HEK 293 T cells using an anti-His antibody (Novagen, 1/1000) and a Alexa Fluor 647-conjugated goat anti-mouse IgG antibody (H+L) (Invitrogen, 1/300) (Supplementary Figure 2A). The quality of Nb-A1 and azide-Nb-A1 productions was evaluated using SDS PAGE (4–12%) electrophoresis and revelation with an anti-His antibody (Novagen, 1/1000) (Supplementary Figure 2B).

Conjugation of Nanobody A1 to the NA

NA were functionalized with nanobody A1[25] described above by click chemistry with the DBCO linker on the surface of the NA. Thirty minutes prior to each experiment the volume of stock NA necessary for the experiment was mixed with the nanobody and incubated 30 min at room temperature with shaking to enable the coupling. As an example, for 1 µL of NA (corresponding to 9.2×10^6 NA) the optimal coupling ratio, determined experimentally by flow cytometry, was obtained with the addition of 15.1 ng of nanobody (corresponding to 1.2×10^{-15} moles). The resulting targeted NA will be named FONmagc-Nb in this article. FONmagc-Nb were either used immediately or stored for several days at 4°C before utilization, without any impact on the results.

Viability Assay

Cell lines were seeded at 5 000 cells/well in a flat bottom 96 wells culture plate in 180 µL of culture medium. The next day, serial dilutions (20 µL) of NA were added to the wells and cells were further incubated for 72 h at 37°C. The viability was assessed using the CellTiter-Glo Luminescent Cell Viability Assay (Promega G7570).

Flow Cytometry

MSLN Staining of Meso34 and Meso34-MSLN Cell Lines

Cells (100 000 cells/condition) were stained in suspension for 30 min at 4°C with 1 µg/mL of a PE conjugated anti-human MSLN antibody (R&D Systems FAB32652P). Cells were washed twice with PBS and analyzed by flow cytometry (ex 488 nm/em 585 nm) on a BD FACSCanto II.

NA Binding to MSLN

Cells (100 000 cells/condition) were stained in suspension for 30 min at 4°C with 25 µL of NA (corresponding to 2.3×10^8 NA) diluted in 25 µL of PBS. Cells were washed twice with PBS and analyzed by flow cytometry (ex 488 nm/em 780 nm) on a BD FACSCanto II.

Internalization Kinetics

All cell lines were seeded at 50 000 cells/well in 12 wells plates in 1 mL of culture medium. The next day, 40 µL of NA (corresponding to 3.7×10^8 NA) were added directly into each well. After 3, 6, 24 or 48 h of incubation at 37°C cells were washed with PBS, harvested by trypsin digestion and analyzed by flow cytometry (ex 488 nm/em 780 nm) on a BD FACSCanto II.

Endocytosis Inhibitors

Meso34-MSLN cells were seeded at 25 000 cells/well in 24 wells plates in 0.5 mL of culture medium and incubated overnight at 37°C. The next day, cells were pre-treated with cytochalasin D (5 µM, Sigma-Aldrich C8273), chloroquine (50 µM, Sigma-Aldrich C6628), dynasore (100 µM, Sigma-Aldrich 324,410), or left untreated for the controls during 1 h at 37°C before addition of 20 µL of FONmagc-Nb/well (corresponding to 1.8×10^8 NA). For the 4°C condition, the plates were pre-incubated at 4°C for 30 minutes before addition of the NA. Cells were incubated for 3 additional hours with the NA at either 37°C or at 4°C and cells were washed with PBS, harvested by trypsin digestion and analyzed by flow cytometry (ex 488 nm/em 585 nm) on a BD FACSCanto II. As a control, the cytotoxicity of the endocytosis inhibitors on Meso34-MSLN cells was assessed in parallel using the CellTiter-Glo Luminescent Cell Viability Assay (Promega G7570) (Supplementary Figure 1C).

Median fluorescence intensities measured in flow cytometry experiments are normalized on the untreated cells and are displayed as ratios of median fluorescence intensities (RMFI) ± standard error of the mean (SEM).

Confocal Microscopy

Cocultures

For static experiments, Meso34-MSLN-GFP cells were seeded with non-fluorescent Meso34 cells (50:50 ratio) in 8 wells IbidiTreat slides at 30 000 total cells/well in 200 µL of medium and incubated overnight at 37°C. The next day, 20 µL of FONmagc-Nb were added per well (corresponding to 1.8×10^8 NA), and cells were further incubated for 1, 3 or 5 h at 37°C. Cells were washed twice with PBS, fixed with 4% paraformaldehyde (Delta Microscopie GF720170-1010) for 20 min and stained with 5 µg/mL Hoechst 33,342 (Sigma-Aldrich 14,533) for 10 min at room temperature.

For flow culture experiments, Meso34-MSLN-BFP cells were seeded with non-fluorescent Meso34 cells (50:50 ratio) in 6 channels µ-Slide VI 0.4 IbidiTreat flow slides at 200 000 total cells/channel in 200 µL of culture medium and incubated overnight at 37°C. The next day, a 20 µL/min flow of complete RPMI medium containing FONmagc-Nb (2 mL RPMI + 100 µL of NA corresponding to 9.2×10^8 NA) was applied on the cells for 30 min at room temperature. Cells were washed for 30 min with a 20 µL/min flow of PBS, fixed with 4% paraformaldehyde (Delta Microscopie GF720170-1010) for 20 min and stained with 5 µM DRAQ5 (Thermo Scientific 62,251) for 5 min at room temperature. All slides were observed on a Confocal Nikon SIM microscope with a x60 objective.

Internalization

For the internalization kinetics experiment in live microscopy, Meso34-MSLN cells were seeded at 120 000 cells/well in 200 µL of the appropriate medium in a 8 wells IbidiTreat slide and incubated overnight at 37°C. The next day, 20 µL of targeted NA were added per well (corresponding to 1.4×10^8 NA) with 100 nM of SiR-actin-A647 (Spirochrome SC001). The slide was immediately observed on a confocal Nikon FLOV microscope in a 37°C and 5% CO_2 chamber with a x60 objective (images were taken every 10 min for 15 h).

Intracellular Localization

Meso34-MSLN cells were seeded at 120 000 cells/well in 200 µL of the appropriate medium in 8 wells IbidiTreat slides and incubated overnight at 37°C. The next day, 15 µL of FONmagc-Nb were added per well (corresponding to 1.4×10^8 NA), and cells were further incubated for 24 or 48 hours at 37°C. Cells were washed twice with PBS, fixed with 4% paraformaldehyde (Delta Microscopie GF720170-1010) for 20 min and stained with 5 U/mL A647-phalloidin (Invitrogen A22287) and 5 µg/mL Hoechst 33,342 (Sigma-Aldrich 14,533) in PBS-BSA 1%-Triton 0.5% for 10 min at room temperature. The slides were observed on a confocal Nikon SIM microscope with a x60 objective.

Colocalization with Lysotracker

Meso34-MSLN cells were seeded at 50 000 cells/well in 200 µL of medium in 8 wells IbidiTreat slides and incubated overnight at 37°C. The next day, 50 nM of LysoTracker deep red (Invitrogen L12492) were added to the cultures with 20 µL of FONmagc-Nb per well (corresponding to $1,8x10^8$ NA) and cells were further incubated for 6 or 24 h at 37°C. After these incubations 5 µg/mL of Hoechst 33,342 (Sigma-Aldrich 14,533) were added to the cultures and live cells were immediately analyzed on a Confocal Nikon SIM microscope equipped with a 37°C and 5% CO_2 chamber with a x60 objective.

Spheroids

Meso34-MSLN cells were seeded in Nunclon sphera low adherence 96 well plates at 20 000 cells/well in 180 µL of medium. After a quick centrifugation, the plates were incubated for 72 h at 37°C to enable the formation of spheroids. Twenty microliters of FONmagc-Nb were added per well (corresponding to 1.8×10^8 NA) and incubated with the spheroids for 24 h at 37°C. Spheroids were then harvested, washed twice with PBS, fixed with 4% paraformaldehyde (Delta Microscopie GF720170-1010) for 30 min and stained with 5 µg/mL Hoechst 33,342 (Sigma-Aldrich 14,533) in PBS-Triton 2% (Sigma-Aldrich X100) for 24 h at room temperature. Spheroids were transferred and glued in 8 wells Ibidi slides with Cell-Tak (Corning CLS354240) and observed on a Nikon FLOV confocal microscope with a x25 objective.

Transmission Electron Microscopy

Meso34-MSLN cells were seeded in a 6 well plate at 250 000 cells/well in 2 mL of culture medium and incubated overnight at 37°C. The next day, 200 µL of FONmagc-Nb (corresponding to 1.8×10^9 NA) were added to each well, except the control one, and incubated with the cells for 6 or 24 h. Cells were washed twice with PBS and harvested by trypsin digestion. Cell pellets were fixed in a mix of 4% paraformaldehyde and 1% glutaraldehyde (Sigma-Aldrich) in 0.1 M phosphate buffer (pH 7.3) for at least 2 h, washed in phosphate-buffer and post-fixed by incubation with 2% osmium tetroxide (Sigma-Aldrich O5500) for 1 h. Samples were fully dehydrated in a graded series of ethanol solutions and embedded in Epon resin (Fisher scientific, NC9925769), which was allowed to polymerize for 48 h at 60°C. Ultra-thin sections of these blocks were obtained with an ultramicrotome (LEICA Ultracut). Sections were stained with 5% uranyl acetate and 5% lead citrate and observed on a JEOL JEM-1400 Plus microscope (120 kV) equipped with a GATAN OneView camera.

Statistical Analysis

Data are presented as medians ± Standard Error of the Mean (SEM). Medians of two groups were compared using non-parametric Mann–Whitney test. Medians of more than two groups were compared with Kruskal Wallis test. * $p<0.05$, ** $p<0.001$, *** $p<0.001$. All statistical analyses were conducted using GraphPad Prism 10.

Results

Generation of Bioconjugated Nanoassemblies for Mesothelin Recognition

It has previously been reported that actively targeted nanoparticles can enhance the efficacy of anti-cancer drugs by increasing their concentration in tumor cells, protecting the cargo from degradation or titration by other organs, preventing multidrug resistance establishment and avoiding side effects.[6] We previously designed fluorescent organic NA,[27] named

FONmag, that are composed of iron oxide nanoparticles coating a fluorescent organic core made of self-assembled fluorophores (Figure 1A). We further grafted on FONmag surface a pegylated linker terminated with a dibenzylcyclooctyne (DBCO) moiety (NA named FONmagc in the text) to easily couple a targeting agent through click chemistry and impart the latter with enough mobility to adapt its target (Figure 1A). In this study, a nanobody targeting human MSLN tumor antigen[25] was chosen to enable tumor targeting of MSLN+ cancer cells (NA named FONmagc-Nb in the text). Transmission electron microscopy, albeit precluded for the final bioconjugated NA due to the presence of salts, revealed well-defined spherical NA with a dry diameter of less than 80 nm, as usually observed after loss of the hydration shell under vacuum (Figure 1B). During successive functionalization, a slight increase in the Z-average hydrodynamic diameter D_Z (from 175 ± 73 nm before PEG grafting to 199 ± 89 nm for the final clickable NA) could be noticed by dynamic light scattering (DLS) as a result of a more extended hydration shell upon introduction of polar and ionic moieties (Figure 1C and Table 1). The apparently larger diameter from the DLS-intensity mode may be relative to reversible internanoparticle chaining as evidenced by TEM imaging revealing some agglomerates. Besides the slight size evolution, the NA absorption and emission properties also displayed detectable changes that are typical of their surface modification.[30] For the sake of clarity, absorption spectra were normalized regarding the band in the visible range, centered at 480 nm. The large increase in the UV range, below 300 nm, was ascribed to DBCO absorption, thereby proving the introduction of the clickable agent. Interestingly, the emission spectrum of the initial FONmag NA underwent a small hypsochromic shift from 627 to 622 nm after introducing the whole DBCO terminated-linker (Figure 1D). Additionally, the substantial increase in the fluorescence

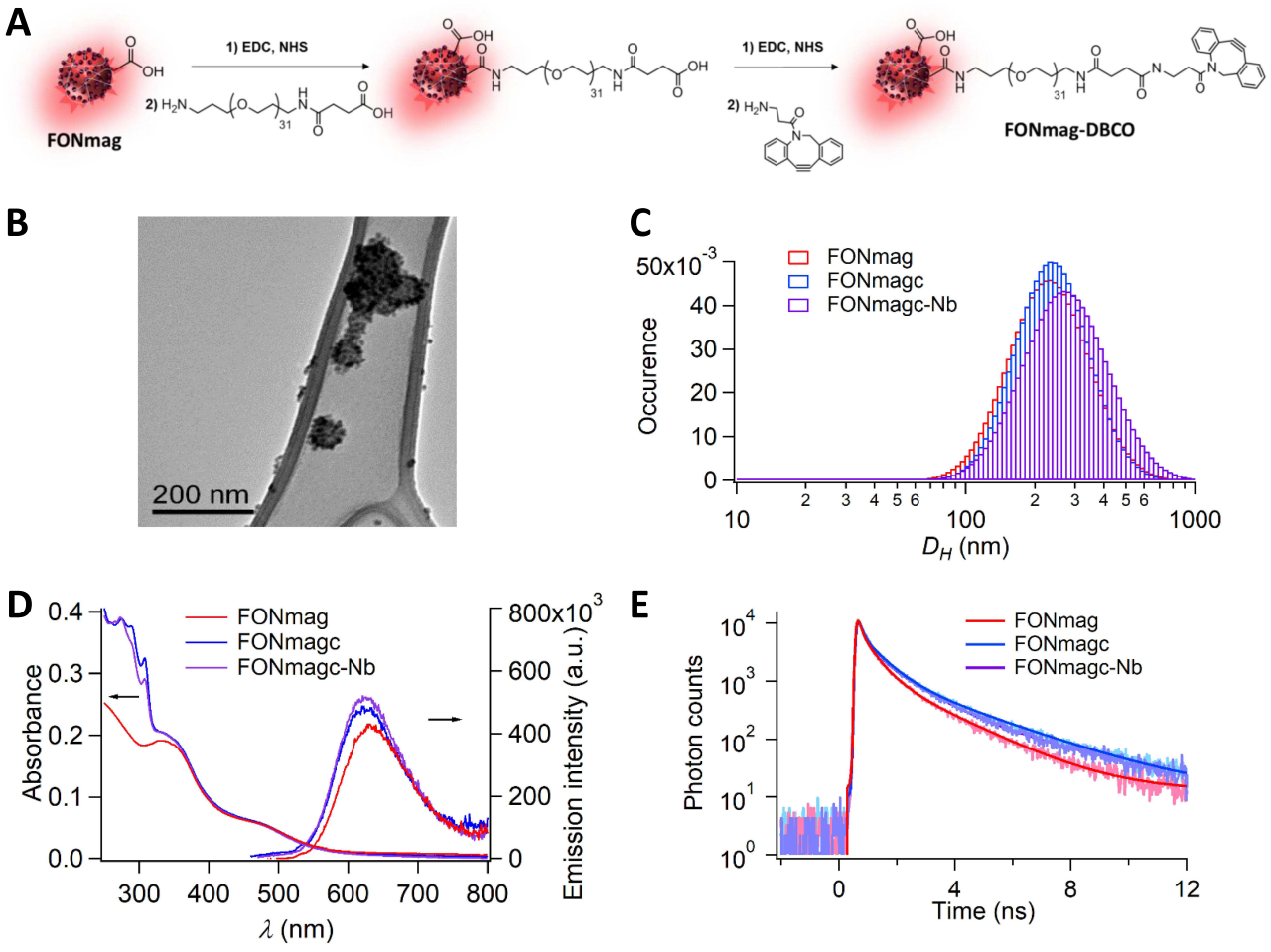

Figure 1 FONmag and nanoassembly derivatives upon functionalization. (**A**) Schematic synthetic pathways. (**B**) Transmission electron microscopy imaging on holey carbon-coated copper grids of FONmag and DBCO-functionalized (FONmagc) NA. (**C**) DLS measurements in aqueous dispersions. (**D**) UV-vis absorption and emission (λexc = 480 nm) spectra in water. (**E**) Fluorescence time decays (λexc = 480 nm and λem = 630 nm) in water of FONmag, FONmagc and FONmagc-Nb nanoassemblies.

Table 1 Structural and Photophysical Characteristics of Functionalized Magneto-Fluorescent Nanoassemblies in Water

NA	D_Z (nm)[a]	PDI	z (mV)[c]	I_{max}(em) (nm)[a]	F_f (×10^{-2})[b]	(ns)[c]
FONmag	175 ± 73	0.18	−22 ± 3	627	0.69	1.00
FONmagc	187 ± 71	0.14	−15 ± 2	622	0.75	1.28
FONmagc-Nb	199 ± 89	0.20	−25 ± 2	622	0.78	1.30

Notes: [a]Upon excitation at 460 nm. [b]Coumarin 540A in ethanol as a fluorescence standard (F_f =0.38).[c]Intensity-weighted average lifetime calculated after reconvolution considering the 450 nm excitation pulse (< 70 ps fwhm).

quantum yield by 9% (from 6.9×10^{-3} for FONmag to 7.5×10^{-3} for the final clickable NA), accompanied by longer fluorescence time decays for clickable NA (Figure 1E and Table 1) could be noticed. We also measured a decrease in the zeta surface potential ζ from −22 ± 3 mV for FONmag NA to −15 ± 2 mV DBCO-functionalized NA (Table 1).

Specific Binding of FONmagc-Nb to MSLN+ Cancer Cells

The next question was to assess the capacity of FONmagc-Nb to bind to their target antigen on the surface of tumor cells. To answer this question, we used two pleural mesothelioma cell lines: Meso34, from our biocollection of MPM cells, that express very low levels of MSLN, and the same cell line transduced to overexpress MSLN (Meso34-MSLN) (Supplementary Figure 3A and B). We first evaluated the natural toxicity of FONmagc-Nb on these two cell lines. The viability of both cell lines remained unchanged, even in the presence of high amounts of FONmagc-Nb NA after 72 h of incubation, thus suggesting the absence of intrinsic toxicity of the two types of NA (Figure 2A). To test the capacity of the NA to bind to the cell surface, we next incubated the two cell lines with FONmagc or FONmagc-Nb, and NA binding was measured by flow cytometry. FONmagc were only able to weakly bind to the two cell lines, regardless of MSLN expression (Figure 2B). FONmagc-Nb were able to bind in a significantly larger amount to Meso34-MSLN cells than to Meso34 cells. In this experiment, the fraction of Meso34-MSLN cells labeled with FONmagc-Nb represented approximately 65% of the total cell population, whereas the proportion of cells labeled with FONmagc was less than 10% (Supplementary Figure 3C and D). This result confirms the presence and the functionality of the nanobody on the surface of FONmagc-Nb NA. To assess the specificity of FONmagc-Nb for MSLN expressing cells, we incubated cocultures of Meso34-MSLN cells expressing cytoplasmic GFP (Meso34 MSLN/GFP) and non-fluorescent Meso34 cells (MSLN-) with FONmagc-Nb for 1, 3 or 5 h (Figure 2C). The specific binding of NA to MSLN was studied using confocal microscopy. We noticed an enrichment of FONmagc-Nb signal in Meso34 MSLN/GFP cells over time, illustrated by the presence of a high number of yellow dots (NA) in green-fluorescent cells after 5 h of incubation (Figure 2C, merge picture). By contrast, we only observed a small number of yellow dots in Meso34 cells of the coculture (visible by their blue nucleus) (Figure 2C, merge picture). This result demonstrates the selectivity of FONmagc-Nb for MSLN expressing cells even in a mixed environment of MSLN+ and MSLN- cells.

Impact of the Functionalization of FONmagc on NA Internalization by Cancer Cells

We studied the functional impact of the active targeting of NA on their internalization by cancer cells. To answer this question, we monitored NA internalization kinetics by flow cytometry, where the cellular fluorescence signal mostly corresponds to NA internalized by cancer cells. No difference was observed between the internalization kinetics of FONmagc and FONmagc-Nb on Meso34 cells (Figure 3A). However, we obtained a faster and stronger internalization of FONmagc-Nb by Meso34-MSLN cells compared to FONmagc NA (Figure 3B). In addition, a significantly higher number of NA, corresponding to yellow dots, was also noticed in Meso34-MSLN cells incubated with FONmagc-Nb for 15 h compared to Meso34-MSLN cells incubated with FONmagc in confocal microscopy (Supplementary Figure 3E and F). This enrichment of FONmagc-Nb in MSLN+ MPM cells over time was further confirmed by live imaging in confocal microscopy (Figure 3C). This set of data suggests that the addition of the nanobody is able to stimulate NA internalization specifically by MSLN expressing MPM cells. To demonstrate the ability of FONmagc-Nb to also bind to cells expressing endogenous levels of MSLN, we used three additional cell lines: Meso13 (an MPM cell line), A1847 (an ovarian carcinoma

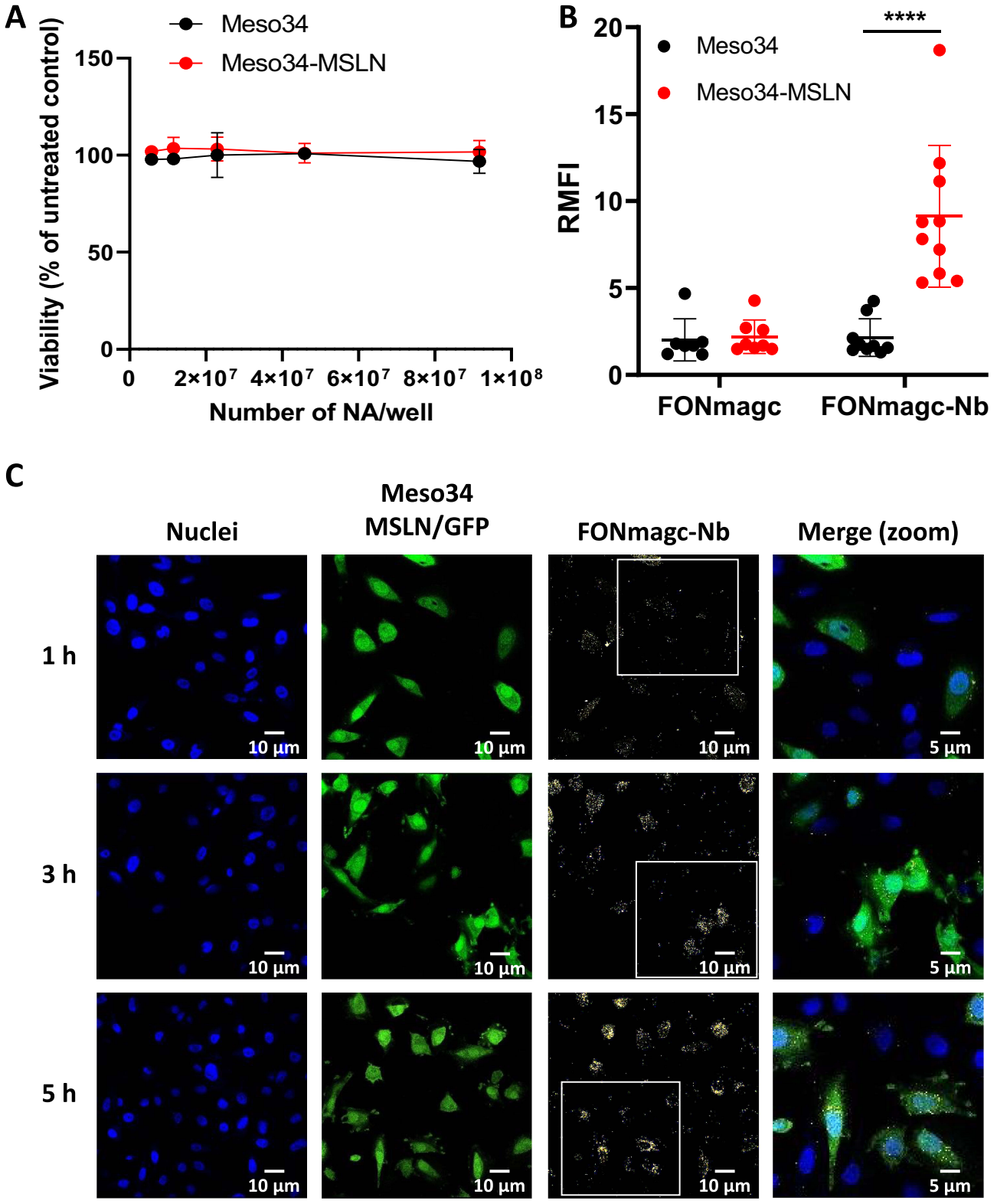

Figure 2 FONmagc-Nb nanoassemblies can specifically bind to cellular mesothelin. (**A**) FONmagc-Nb were incubated with MSLN-expressing MPM cells (Meso34-MSLN) or control MPM cells (Meso34) for 72 h and cell viability was assessed by bioluminescence to determine the toxicity of the NA. The graph shows the means ± SEM of 3 independent experiments. (**B**) MSLN-expressing MPM cells (Meso34-MSLN) or control MPM cells (Meso34) were stained with FONmagc or FONmagc-Nb for 30 min at 4°C. Specific fixation of the fluorescent NA to mesothelin was measured by flow cytometry (n=10) and is represented as RMFI ± SEM. Mann–Whitney, **** p<0.0001. (**C**) Fluorescent MPM cells expressing mesothelin (Meso34-MSLN) were cocultured (50/50) with unstained control MPM cells (Meso34) that do not express mesothelin. Mesothelin-specific binding of FONmagc-Nb was assessed at several time points by confocal microscopy (representative images, x60 obj).

cell line) and ADCA153 (a lung adenocarcinoma cell line). The endogenous level of MSLN expression of these cell lines was assessed by flow cytometry (Figure 3D) and we compared to the capacity of the cells to internalize FONmagc and FONmagc-Nb NA (Figure 3E). We first noticed that the level of MSLN is heterogeneous between cell lines and overall lower than that of Meso34-MSLN (Figure 3D). We observed that the fluorescence signal obtained with FONmagc-Nb is always significantly higher than that obtained with FONmagc (Figure 3E). This result suggests that the functionalization of FONmagc with the nanobody also enables the recognition of endogenous expression of MSLN on cancer cells. However, even though the addition of the nanobody on NA increased their binding to all cell lines, the intensity of the fluorescent

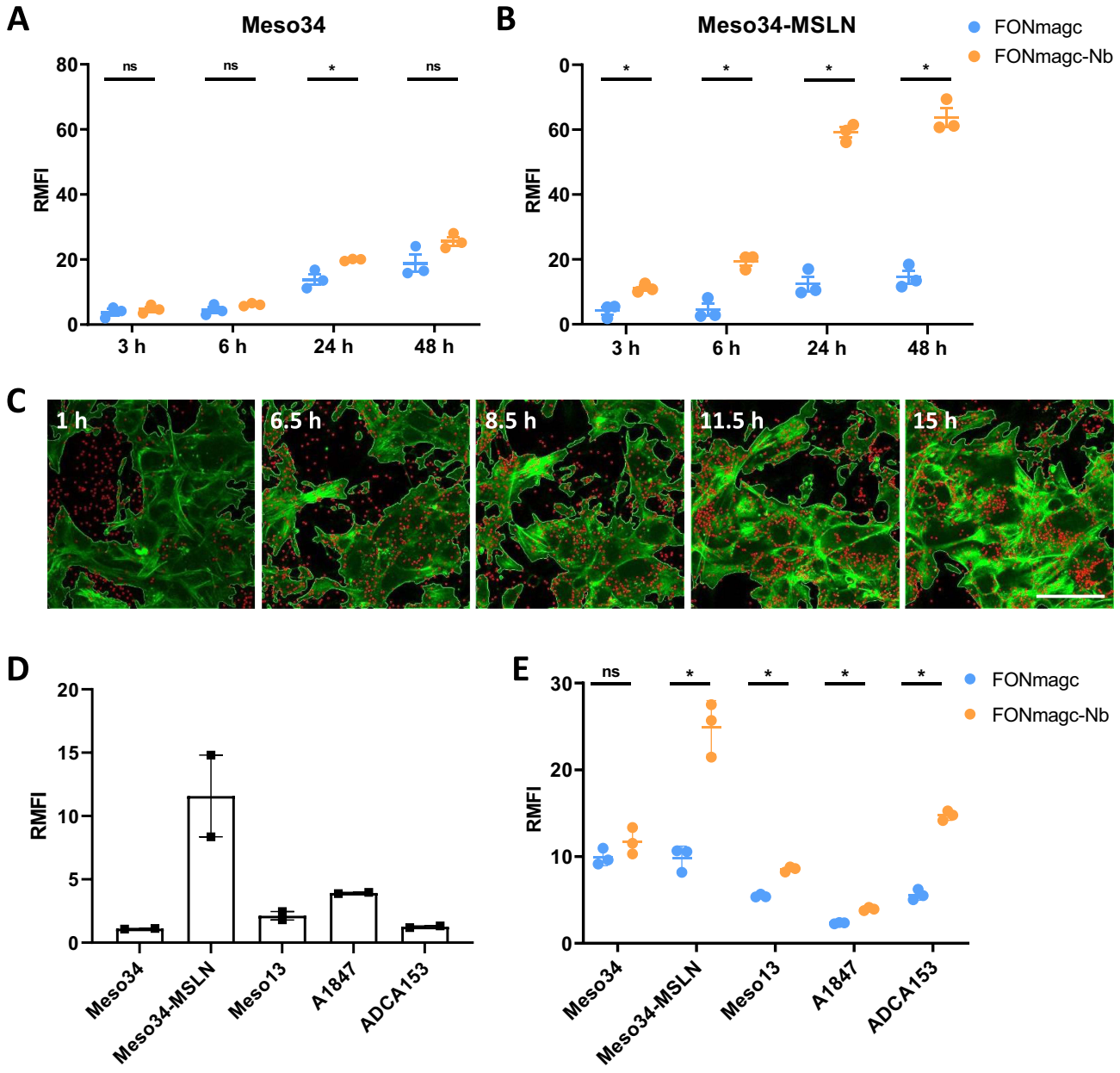

Figure 3 Internalization of FONmagc-Nb is enhanced in MSLN expressing cancer cell lines. (**A** and **B**) FONmagc or FONmagc-Nb were incubated with MSLN- (**A**) or MSLN+ (**B**) MPM cells at 37°C for several hours. At each time point cells were washed, harvested and cellular fluorescence corresponding to internalized NA was analyzed by flow cytometry (n=3). Results correspond to RMFI ± SEM. Mann–Whitney, ns: non-significant, *p<0.05. (**C**) FONmagc-Nb were added on MSLN overexpressing MPM cells (Meso34-MSLN) and their internalization was followed over time using confocal microscopy in live cells with an actin staining (x60 objective). Pictures show middle slices of representative time points after cell contouring and NA tracking (red circles) on the NIS/GA3 software. Scale bar = 50 µm. (**D**) Several cancer cell lines were stained with an anti-MSLN antibody to determine endogenous MSLN expression level on the surface of the cells (n=2). Results are represented as RMFI ± SEM. (**E**) FONmagc or FONmagc-Nb were incubated with the cancer cell lines shown in (**D**) at 37°C for 24 h. Cells were washed, harvested and cellular fluorescence corresponding to internalized NA was analyzed by flow cytometry (n=3). Results are represented as RMFI ± SEM. One-tailed Mann–Whitney, ns: non-significant, *p<0.05.

signal was not fully correlated with MSLN expression levels on the cells. Indeed, whereas the expression of MSLN was lower in ADCA153 cell line than in A1847 cell line, the internalization of FONmagc-Nb by ADCA153 cells was higher than in A1847 cells after 24 h of incubation. The internalization rate of the NA thus seems to be dependent on both the presence of MSLN and the cancer cell type.

Characterization of NA Endocytosis in MSLN+ Cancer Cells

In order to confirm the internalization and study the intracellular localization of FONmagc-Nb inside the cells, we used confocal microscopy. Using actin staining (purple), we showed the presence of FONmagc-Nb (yellow dots) in the cytoplasm, but not in the nucleus (blue), of Meso34-MSLN cells after 24 h and 48 h of incubation (Figure 4A). Internalization mechanisms are dependent on the type of interactions between nanoparticles and the cellular membrane. Thus, we used several endocytosis inhibitors to characterize the endocytic pathways used by MSLN+ cancer cells to enable NA internalization.[31] Pitstop 2 and chloroquine can block clathrin-mediated endocytosis, whereas dynasore inhibits dynamin-dependent endocytosis pathways and cytochalasin D inhibits the remodeling of actin cytoskeleton. The strongest inhibition of NA internalization was obtained by incubating the cells at 4°C (approximately 80% of inhibition), showing that this internalization process requires an active mechanism (Figure 4B). We also obtained a decrease by around 40% of the fluorescent signal in cells treated with dynasore. Several mechanisms are probably simultaneously operating to enable the internalization of these NA, but they appear at least clathrin-independent, energy-dependent and partially dynamin-dependent. To go further, we also performed transmission electron microscopy (TEM) imaging of Meso34-MSLN, 6 and 24 hours after addition of NA in the culture medium. NA were clearly visible inside the tumor cells at the two time points (Figure 4C). In some pictures, NA were observed at the plasma membrane, in the vicinity of clathrin coated pits (Figure 4C, indicated by a white arrowhead), but in most instances NA appeared inside intracellular vesicles. At the early time point, NA were mostly found in single membrane compartments with electron-lucent content compatible with endosomes (Figure 4C, indicated by a black arrow and the letter E). In some instances, they were also found in single membrane compartments with heterogenous electron-dense content compatible with lysosomes (Figure 4C, indicated by a black arrow and the letter L). At 24 h, the majority of NA seemed to be located in multi-membrane compartments with electron-dense content compatible with autophagolysosomes (Figure 4C, indicated by a black arrow and the letter A). To confirm the presence of NA in intracellular acidic compartments, we studied FONmagc-Nb intracellular localization after 6 and 24 h of incubation with Meso34-MSLN cells using an acido-sensitive dye and confocal microscopy (Figure 4D and 4E). After 6 h of incubation, only 5% of the NA signal seemed to colocalized with acidic compartments (probably lysosomes) whereas we obtained around 60% of colocalization of NA and lysosome signal after 24 h of incubation (Figure 4D). In Figure 4E, the colocalization of FONmagc-Nb with lysosomes is illustrated by the superposition of the yellow dots (NA) with the red signal (lysosomes) resulting in an orange color on the merge. These results were coherent with those obtained by TEM and suggest that most part of FONmagc-Nb end up in endo-lysosomal degradation structures after internalization by Meso34-MSLN MPM cells.

Behavior of FONmagc-Nb in Models Mimicking MPM Pathophysiological Conditions

With the aim to be closer to pathophysiological conditions in tumors, we also studied the capacity of FONmagc-Nb to bind to the surface of multicellular tumor spheroids (MCTS) of Meso34-MSLN cells. Three days MCTS were incubated for 24 h with FONmagc-Nb, and the diffusion properties of NA were assessed by confocal microscopy. As shown in Figure 5A, NA (yellow signal) were able to enter the first cellular layers of MCTS. A large amount of NA was visible inside the cells of the superficial layers of the spheroids. However, the most internal layers appeared inaccessible to the NA. Results were similar with FONmagc NA, suggesting that the addition of the nanobody does not modify diffusion properties of the NA (Supplementary Figure 4). With the same goal to mimic physical constraints in tumors, we also studied the capacity of FONmagc-Nb to bind to Meso34-MSLN cells under dynamic culture conditions. Indeed, in the case of MPM, therapies can be directly administrated in the pleural cavity where the pleural fluid is perpetually moving due to the breathing of the patient, generating hydrodynamic constraints in the pleural cavity. Thus, we applied a flow of culture medium containing FONmagc-Nb for 30 minutes on a coculture of fluorescent MSLN+ (Meso34 MSLN/BFP) and non-fluorescent MSLN-cancer cells (Meso34), and studied NA binding by confocal microscopy. In these dynamic

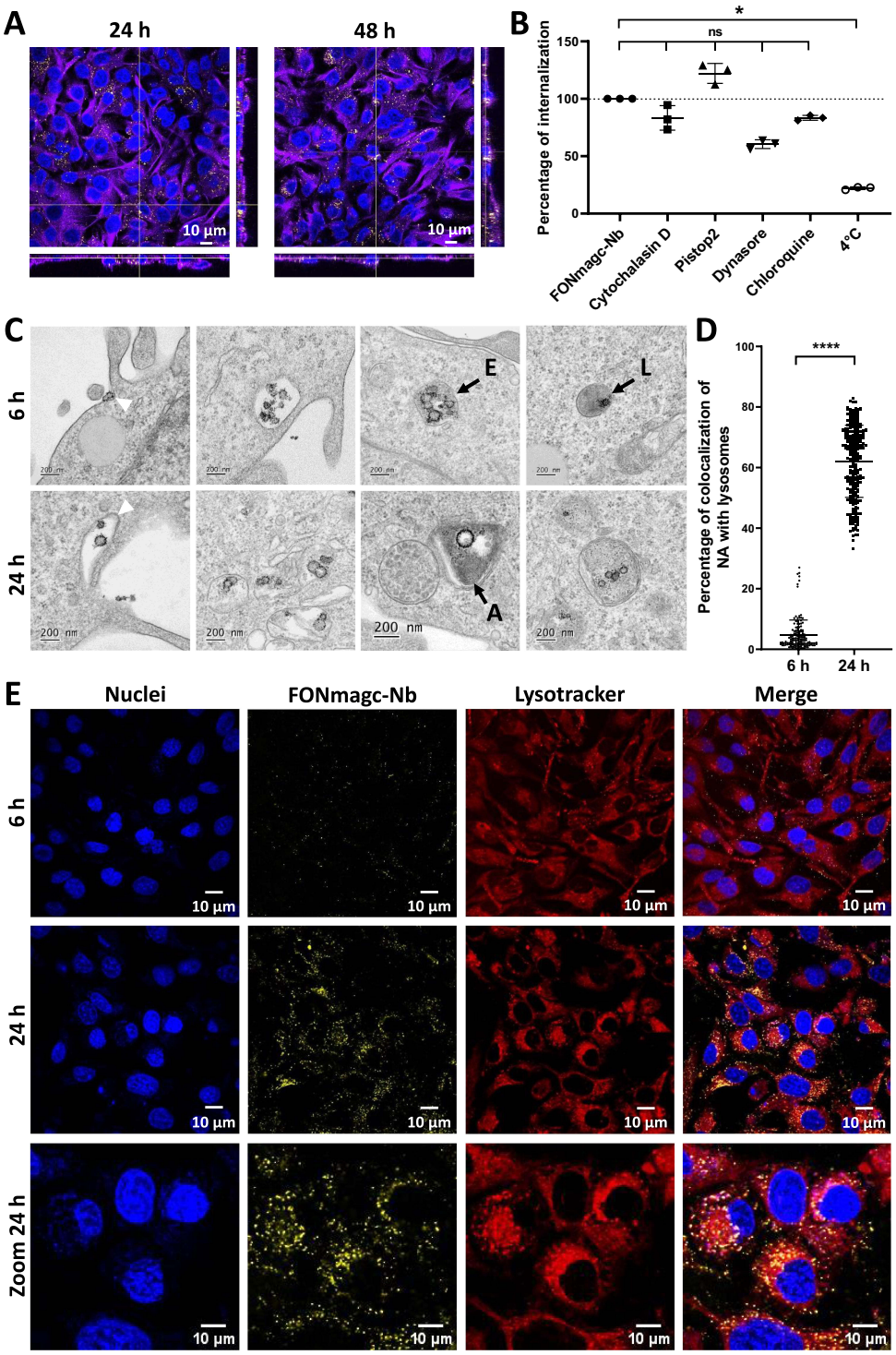

Figure 4 FONmagc-Nb are internalized by an energy- and dynamin-dependent pathway in MSLN+ cancer cells and end up their course in intracellular degradation vesicles. (**A**) Mesothelin expressing MPM cells (Meso34-MSLN) were incubated for 24 or 48 h at 37°C with FONmagc-Nb. Internalization of the NA was visualized by confocal microscopy (x60 obj.) and is presented as orthogonal views. Blue = nuclei; purple = phalloidin; yellow = FONmagc-Nb. (**B**) Meso34-MSLN cells were pre-treated for 1 h with several endocytosis inhibitors, left untreated or incubated at 4°C. FONmagc-Nb were added to the cultures and incubated with the cells for 3 h at 37°C or 4°C before the cells were washed, harvested and analyzed by flow cytometry (n=3). The graphic presents the fluorescence percentage ± SEM for each condition compared to untreated cells incubated with FONmagc-Nb at 37°C. Kruskal Wallis, ns: non-significant, *p<0.05. (**C**) Meso34-MSLN cells were incubated for 6 or 24 h at 37°C with FONmagc-Nb NA and analyzed by transmission electron microscopy after negative staining to visualize NA internalization. White arrowheads, at 6 h the interaction of the NA with the plasma membrane, at 24 h a clathrin coated pit. E = endosome; L = lysosome. (**D** and **E**) FONmagc-Nb were incubated with Meso34-MSLN MPM cells for 6 or 24 h at 37°C. Cells were then stained with a lysotracker fluorescent probe and the colocalization of stained endo-lysosomes and internalized NA was evaluated on live cells by confocal microscopy (x60 obj.). The quantification of the colocalization realized on Fiji (corresponding to 50 cells) is presented in (**D**) and representative images are displayed in (**E**). Unpaired *T*-test, ****p<0.0001.

conditions, FONmagc-Nb bound almost exclusively to MSLN+ cells, as illustrated by the presence of yellow dots on blue-fluorescent cells but not on non-fluorescent cells (visible by their purple nucleus), confirming the specificity of FONmagc-Nb and their efficiency to target MSLN+ cells (Figure 5B).

Discussion

MPM is a rare but particularly aggressive incurable disease for which current treatments are only palliative. However, the MSLN tumor antigen appears to be a prime candidate for MPM targeted therapy. Indeed, a lot of therapeutic strategies targeting MSLN are currently evaluated in clinical trials with limited but encouraging efficiencies, offering great hopes for the future management of this cancer. In this study, we aimed at designing hybrid fluorescent NA, with multimodal imaging properties, functionalized with a nanobody to enable the targeting of MSLN-expressing cells. We first showed the non-toxicity of our systems and confirmed that NA actively targeted against MSLN were able to specifically bind to and to be internalized by MSLN expressing MPM cells. The active targeting of the NA led to an acceleration in the internalization kinetics of the NA in MSLN+ cancer cells and promoted the accumulation of the NA specifically in these cells. This internalization process appeared to require, at least partially, a dynamin activity and ATP. We also demonstrated that the targeted NA localized in intracellular degradation structures, such as mature lysosomes, 24 h after endocytosis. Finally, we also showed that targeted NA are able to enter the most superficial layers of MSLN+ multicellular tumor spheroids and to bind to their targets even in the presence of a flow to mimic hydrodynamic constraints in the pleural cavity.

Several nanodrugs have already been approved to treat solid cancers, such as Doxil (Pegylated liposomal doxorubicin) and Abraxane (Paclitaxel bound to albumin nanoparticles), and hopefully more will come soon.[32] All of them are however passively targeted nanosystems. The main benefit of therapeutic nanovectorization noted in patients is a decrease of the toxicity of vectorized molecules, compared to injections of the corresponding free molecules. Unfortunately, no significant improvement of overall survival of patients was noticed in clinical trials so far. However, in a phase II clinical trial conducted in MPM, the tumoral accumulation of liposomal doxorubicin, although being a rare event, was associated with a better survival of patients.[8] This observation supports the interest of adding a targeting agent to the surface of nanodrugs to increase even more the accumulation of anti-cancer molecules in tumors.

One of the reasons why targeted nanovectors have failed to reach approval so far is because they display a complex structure that drives safety issues.[33] Nevertheless, active targeting, while adding complexity for drug development, is now considered essential to further improve the efficacy and the selectivity of treatments.[6] As mentioned in the literature, the optimal nanovector size range for reaching tumor enrichment is 20 to 200 nm.[6,34] Surface chemistry and charge also play an important role in their biodistribution and in their interactions with cells.[35] Indeed, negatively charged nanocarriers have been described to enter tumor cells slower than positively charged nanocarriers because of electrostatic repulsions with the negatively charged cell membrane. However, positively charged nanovectors tend to generate cytotoxicity because of membrane depolarization.[36] FONmagc-Nb display an average hydrodynamic diameter of 199 ± 89 nm, a negative surface charge (−25 ± 2 mV) and demonstrated their non-toxicity for MPM cells. Moreover, the slight modifications in the hydrodynamic diameter and emission spectrum of FONmag NA after conjugation of the nanobody tend to point out a slight transformation of the surroundings around the hybrid magneto-fluorescent core, becoming less polar. This is due to the partial transformation of the carboxylate units of the polyacrylate chains coating the surface of FONmag NA, into pegylated chains terminated with a hydrophobic DBCO moiety. This indirectly proves the reality of FONmag surface functionalization that brings additional hydrophobicity and helps to repel water molecules amenable to emission quenching upon hydrogen-bonding.[30] The observation of a more pronounced emission enhancement upon grafting the nanobody, along with the decrease of the zeta potential ζ value to −25 mV ± 2 mV, suggest the trapping of water molecules by the negatively charged nanobodies, which brings additional indirect evidence of the bioconjugation efficacy.

It is now established that the addition of a targeting ligand on nanocarriers increases their cellular internalization by target cells without affecting overall biodistribution.[34,37] Frequently used targeting ligands include high-affinity small molecules, peptides, aptamers, antibodies and antibody fragments.[38] In our study, we decided to use an already characterized nanobody directed against MSLN to functionalize FONmag NA.[25] Nanobodies are currently developed as drug-conjugates, radionuclide vectors, CAR T cells or anti-tumor vaccines for cancer imaging or therapy applications.[39] They usually combine a high affinity with a small size limiting steric hindrance on the surface of the NA to enable good mobility and functionality of the targeting agent.[40–42] Moreover, nanobodies are recognized to be more stable and soluble than scFvs, their conventional antibody-

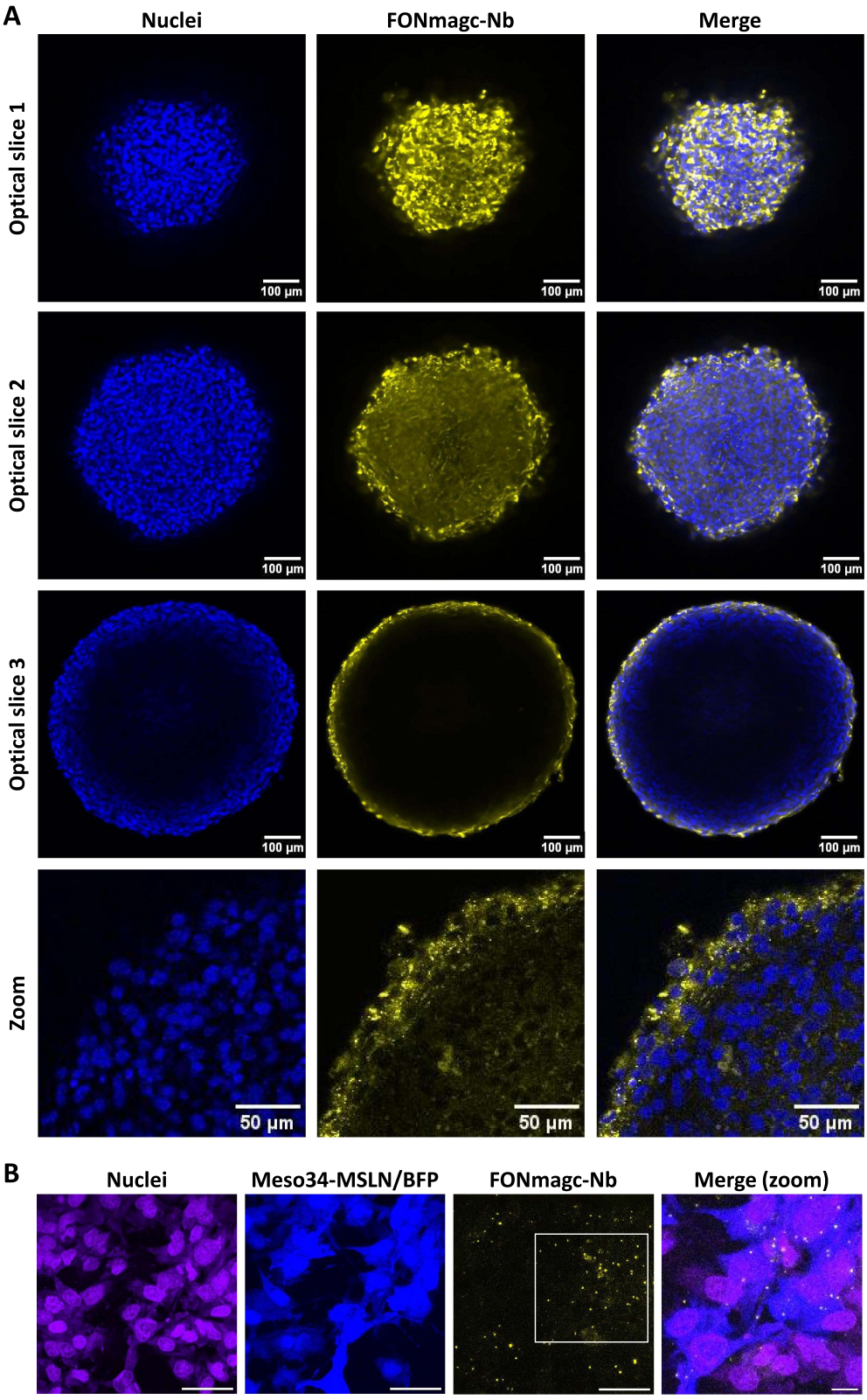

Figure 5 Assessment of FONmagc-Nb behavior in complex culture models, closer to pathophysiological conditions in tumors. (**A**) FONmagc-Nb were added on pre-formed multicellular tumor spheroids of MPM cells expressing MSLN for 24 h at 37°C. The penetration of the NA in the 3D structures was assessed by confocal microscopy after transparization and nuclei staining (x25 obj). Blue: nuclei; yellow: FONmagc-Nb. (**B**) A flow of culture medium containing FONmagc-Nb was applied on a coculture of blue-fluorescent Meso34-MSLN (MSLN+) and non-fluorescent Meso34 (MSLN-) cancer cells for 30 min. Specificity of NA binding was then assessed by confocal microscopy (x60 obj) after Draq5 nuclei staining. Scale bar = 50 µm. Blue: Meso34-MSLN cells; purple: nuclei, Yellow: FONmagc-Nb.

derived counterparts, because they lack hydrophobic regions typical of conventional antibodies.[40,43,44] Finally, the constant regions of immunoglobulins are known to be highly immunogenic across species, whereas responses against their variable domains are much less frequent.[40] Nanobodies typically display high similarities with human type 3 VH domains (VH3), likely accounting for their low immunogenicity,[45] and several clinical trials have demonstrated their minimal immunogenicity.[45,46] They are thus considered advantageous for the functionalization of nanocarriers as their low immunogenicity delays the clearance of the nanobody-targeted nanocarriers from the body.[40] We showed that using a nanobody for the targeting of FONmag NA enables a specific binding of the targeted NA on MSLN+ cancer cells and the efficient triggering of a receptor mediated endocytosis. We also demonstrated a significant increase of the internalization rate of targeted FONmag in MSLN expressing MPM cells compared to untargeted FONmag, leading to an overall larger accumulation of targeted NA in MSLN+ cancer cells after 24 and 48 h of incubation. MSLN active targeting allowed us to correct the lack of tumor specificity of FONmag NA while promoting their accumulation in MSLN+ cancer cells over time, even in coculture models.

We showed that bioconjugated FONmag trigger an energy-dependent endocytosis pathway that is not impacted by pitstop2 and chloroquine, two inhibitors known to inhibit mostly clathrin-mediated endocytosis. This is rather surprising as the majority of receptor-mediated cellular uptake of nanocarriers is usually described to occur through clathrin-mediated endocytosis.[31,47] In contrast, we demonstrated that FONmagc-Nb uptake is partially inhibited by the dynasore inhibitor, suggesting that the endocytosis of targeted FONmag is in part dynamin-dependent. Endocytosis of targeted FONmag thus seems to belong to the clathrin-independent endocytosis family, in the dynamin-dependent subclass. Recent studies suggest that clathrin-independent endocytosis could be a novel mechanism for cellular uptake of nanoparticles.[47] This class of endocytosis was notably found to be dependent on actin filaments and dynamin. However, most of the time, the internalization of a nanocarrier does not rely on a unique endocytosis pathway. It is likely that the majority of targeted FONmag enters MSLN+ MPM cancer cells by a clathrin-independent/dynamin-dependent endocytosis, but a small amount of them probably enters the cells by another mechanism, the most classical being clathrin-dependent endocytosis and macropinocytosis. This hypothesis is supported by the presence of clathrin coated pits near the interaction zone between targeted FONmag and the plasma membrane observed in TEM. Moreover, the cell type is also a criterion likely to affect nanoparticles uptake.[48] It is possible that the endocytosis pathway for targeted FONmag uptake would be different in another MSLN+ cell type, or even in another MPM cell line. As an illustration, we noticed that targeted FONmag cellular uptake in several cancer cell lines not only relies on their MSLN expression level but also on the cancerous origin of the cell line itself.

It is documented that cargos entering cells through clathrin-independent endocytosis are usually delivered to early endosomes that mature into late endosomes and fuse with lysosomes.[47,49] We showed, by confocal microscopy, that 80% of the targeted FONmag localized in acidic intracellular structures 24 h after incubation with MSLN+ MPM cells. This was confirmed by TEM images in which NA were found mostly in immature lysosomes after 6 h of incubation, and in degradation vesicles such as mature lysosomes, autophagolysosomes or multivesicular bodies after 24 h of incubation. This phenomenon is classical for nanoparticles and could be exploited to deliver therapeutic agents, given that we already demonstrated the importance of these acidic compartments to induce the degradation and the delivery of molecules by FONmag NA.[24,50]

Constraints related to the 3D structure of tumors are usually poorly integrated in the in vitro evaluation of a therapy.[37] For MPM, local injections of treatments into the intrapleural space enable direct access to malignant cells and are already performed in the clinic, allowing to avoid some cellular barriers and clearance associated with systemic injections.[51] However, the pleural space contains a fluid, and therapies injected in this area are submitted to hydrodynamic constraints related to breathing and movements of patients. To mimic these situations, we used MPM cells cultured as MCTS or under a flow of culture medium. We showed that targeted FONmag NA were able to enter the superficial layers of these MCTS, as FONmagc and as previously observed with non-targeted FONmag NA.[30,52] This suggests that the addition of the nanobody on the surface of FONmag did not alter their diffusion properties in a complex environment such as MCTS. We also observed that the application of a flow did not alter the specific recognition of target cells by bioconjugated FONmagc-Nb NA. Therefore, the designed NA seem to have the required properties for considering future applications in the targeted treatment of MPM using the intrapleural route.

Conclusion

We developed a new targetable fluorescent organic nano-platform for the coupling of targeting agents using copper-free click chemistry. In addition, we propose fluorescent biodegradable NA actively targeting the human MSLN tumor

associated antigen. We demonstrated that these NA can specifically bind to MSLN-expressing cancer cells in coculture, 3D and dynamic culture models. Active targeting of these systems triggered an acceleration of their internalization rate and their specific accumulation in MSLN+ cancer cells. Hence, our study targeting MSLN, an antigen broadly over-expressed on the surface of many cancer types, open attractive prospects to specifically and locally deliver high quantities of drugs using smart bioconjugated NA with enhanced drug delivery capabilities.

Abbreviations

2D, Two dimensions; 3D, Three dimensions; ADCA, Adenocarcinoma cell line; BFP, Blue Fluorescent Protein; BSA, Bovine Serum Albumin; CNIL, Commission Nationale de l'Informatique et des Libertés; DBCO, dibenzocyclooctyne-amine; DLS, Dynamic Light Scattering; D_Z, hydrodynamic diameter; EDC, 1-ethyl-3-(3-dimethylaminopropyl) carbodiimide; GFP, Green Fluorescent Protein; MES, 2-morpholinoethanesulphonic acid; MCTS, MultiCellular Tumor Spheroids; Meso, Mesothelioma cell line; MPM, Malignant Pleural Mesothelioma; MSLN, Mesothelin; NA, nanoassemblies; Nb, nanobody; PBS, Phosphate Buffered Saline; PDI, polydispersity index; RMFI, Ratio of median fluorescence intensity; sulfo-NHS, N-hydroxysulfosuccinimide sodium salt solutions; TAA, Tumor Associated Antigen; TEM, Transmission Electron Microscopy; TRPS, Tunable Resistive Pulse Sensing.

Ethics Approval and Informed Consent

Some cell lines used in this study were established from patient's samples. These samples were collected in accordance with the standards established by the Declaration of Helsinki. All the collected samples and the associated clinical information were registered in database (DC-2011-1399) validated by the French research ministry and Commission Nationale de l'Informatique et des Libertés (CNIL) (n°: 1657097). Study was approved by local ethical committee, CPP Ouest-IV-Nantes (an independent organ from French ministry of health) (n°: 150/2007). All recruited patients gave signed, informed consent.

Data Sharing Statement

The datasets used and analyzed during the current study are available from the corresponding author.

Acknowledgments

The authors thank ARSMeso44 and the cluster LUNG innOvatiOn (LUNG O2) for logistic support. This cluster is supported by the National Research Agency under the Programme d'Investissements d'Avenir (ANR-16-IDEX-0007), the Pays de la Loire Region research program and by the Institut de Recherche en Santé Respiratoire des Pays de la Loire. The authors thank the IBiSA Electron Microscopy Facility of University of Tours and particularly Dr Sebastien Eymieux and Pierre-Yvan Raynal for assistance in TEM analysis. The authors thank the Cytocell core facility for the flow cytometry experiments, the MicroPiCell core facility for microscopy analyses. The authors would also like to thank Sophie Deshayes for her invaluable technical assistance during the revision process.

Author Contributions

All authors made a significant contribution to the work reported, whether that is in the conception, study design, execution, acquisition of data, analysis and interpretation, or in all these areas; took part in drafting, revising or critically reviewing the article; gave final approval of the version to be published; have agreed on the journal to which the article has been submitted; and agree to be accountable for all aspects of the work.

Funding

This work was supported by INSERM, CNRS through its Mission for Interdisciplinary (Nano Challenge/"Health and wellfare" – ETHICAM project), Nantes University (Interdisciplinary programs) and Région des Pays de la Loire ("Paris Scientifiques" program). TB was supported by a fellowship from la Ligue contre le cancer.

Disclosure

Mrs Tina Briolay reports grants from Ligue contre le cancer, grants from INSERM, grants from CNRS, during the conduct of the study. Professor Eléna Ishow reports a patent WO2015/140223 issued to Ishow Eléna, Faucon Adrien, a patent US 9,597,418 issued to Ishow Eléna, Faucon Adrien. Dr Christophe Blanquart reports grants from Ligue contre le cancer, grants from INSERM, grants from CNRS, during the conduct of the study. The authors report no other conflicts of interest in this work.

References

1. Rijavec E, Biello F, Barletta G, Dellepiane C, Genova C. Novel approaches for the treatment of unresectable malignant pleural mesothelioma: a focus on immunotherapy and target therapy (Review). *Mol Clin Oncol*. 2022;16:89.
2. Tsao AS, Pass HI, Rimner A, Mansfield AS. New era for malignant pleural mesothelioma: updates on therapeutic options. *J Clin Oncol off J Am Soc Clin Oncol*. 2022;40:681–692. doi:10.1200/JCO.21.01567
3. Fennell DA, Dulloo S, Harber J. Immunotherapy approaches for malignant pleural mesothelioma. *Nat Rev Clin Oncol*. 2022;19:573–584. doi:10.1038/s41571-022-00649-7
4. Hu ZI, Ghafoor A, Sengupta M, Hassan R. Malignant mesothelioma: advances in immune checkpoint inhibitor and mesothelin-targeted therapies. *Cancer*. 2021;127:1010–1020. doi:10.1002/cncr.33433
5. Baas P, Scherpereel A, Nowak AK, et al. First-line nivolumab plus ipilimumab in unresectable malignant pleural mesothelioma (CheckMate 743): a multicentre, randomised, open-label, Phase 3 trial. *Lancet Lond Engl*. 2021;397:375–386. doi:10.1016/S0140-6736(20)32714-8
6. Briolay T, Petithomme T, Fouet M, et al. Delivery of cancer therapies by synthetic and bio-inspired nanovectors. *Mol Cancer*. 2021;20:55. doi:10.1186/s12943-021-01346-2
7. Arrieta Ó, Medina LA, Estrada-Lobato E, et al. First-line chemotherapy with liposomal doxorubicin plus cisplatin for patients with advanced malignant pleural mesothelioma: phase II trial. *Br J Cancer*. 2012;106:1027–1032. doi:10.1038/bjc.2012.44
8. Arrieta O, Medina LA, Estrada-Lobato E, et al. High liposomal doxorubicin tumour tissue distribution, as determined by radiopharmaceutical labelling with (99m)Tc-LD, is associated with the response and survival of patients with unresectable pleural mesothelioma treated with a combination of liposomal doxorubicin and cisplatin. *Cancer Chemother Pharmacol*. 2014;74:211–215. doi:10.1007/s00280-014-2477-x
9. Sakurai Y, Kato A, Hida Y, et al. Synergistic enhancement of cellular uptake with CD44-expressing malignant pleural mesothelioma by combining cationic liposome and hyaluronic acid-lipid conjugate. *J Pharm Sci*. 2019;108:3218–3224. doi:10.1016/j.xphs.2019.06.012
10. Hassan R, Thomas A, Alewine C, et al. Mesothelin immunotherapy for cancer: ready for prime time? *J Clin Oncol off J Am Soc Clin Oncol*. 2016;34:4171–4179. doi:10.1200/JCO.2016.68.3672
11. Morello A, Sadelain M, Adusumilli PS. Mesothelin-Targeted CARs: driving T Cells to Solid Tumors. *Cancer Discov*. 2016;6:133–146. doi:10.1158/2159-8290.CD-15-0583
12. Weidemann S, Gagelmann P, Gorbokon N, et al. Mesothelin expression in human tumors: a tissue microarray study on 12,679 tumors. *Biomedicines*. 2021;9:397. doi:10.3390/biomedicines9040397
13. Klampatsa A, Dimou V, Albelda SM. Mesothelin-targeted CAR-T cell therapy for solid tumors. *Expert Opin Biol Ther*. 2021;21:473–486. doi:10.1080/14712598.2021.1843628
14. Hagerty BL, Pegna GJ, Xu J, Tai C-H, Alewine C. Mesothelin-targeted recombinant immunotoxins for solid tumors. *Biomolecules*. 2020;10:973. doi:10.3390/biom10070973
15. Zhai X, Mao L, Wu M, Liu J, Yu S. Challenges of anti-mesothelin CAR-T-cell therapy. *Cancers*. 2023;15:1357. doi:10.3390/cancers15051357
16. Cao G, Cao W, Zhang J, et al. Mesothelin targeted nano-system enhanced chemodynamic therapy and tirapazamine chemotherapy via lactate depletion. *Nano Res*. 2023;(5):7108–7118. doi:10.1007/s12274-022-5301-7
17. Conte M, Frantellizzi V, Matto A, De Vincentis G. New insight and future perspective of mesothelin-targeted agents in nuclear medicine. *Clin Transl Imaging*. 2020;8:265–278. doi:10.1007/s40336-020-00379-9
18. Alfaleh MA, Howard CB, Sedliarou I, et al. Targeting mesothelin receptors with drug-loaded bacterial nanocells suppresses human mesothelioma tumour growth in mouse xenograft models. *PLoS One*. 2017;12:e0186137. doi:10.1371/journal.pone.0186137
19. Deng L, Ke X, He Z, et al. A MSLN-targeted multifunctional nanoimmunoliposome for MRI and targeting therapy in pancreatic cancer. *Int J Nanomed*. 2012;7:5053–5065. doi:10.2147/IJN.S34801
20. Tian H, Zhang T, Qin S, et al. Enhancing the therapeutic efficacy of nanoparticles for cancer treatment using versatile targeted strategies. *J Hematol Oncol*. 2022;15:132.
21. Yao Y, Zhou Y, Liu L, et al. Nanoparticle-based drug delivery in cancer therapy and its role in overcoming drug resistance. *Front Mol Biosci*. 2020;7. doi:10.3389/fmolb.2020.00193
22. Mauricio D, Harold J, Tymon-Rosario JR, Zeybek B, Santin AD. Novel mesothelin antibody-drug conjugates: current evidence and future role in the treatment of ovarian cancer. *Expert Opin Biol Ther*. 2021;21:1087–1096. doi:10.1080/14712598.2021.1869210
23. Shen J, Sun X, Zhou J. Insights into the role of mesothelin as a diagnostic and therapeutic target in ovarian carcinoma. *Front Oncol*. 2020;10:1263. doi:10.3389/fonc.2020.01263
24. Boucard J, Linot C, Blondy T, et al. Small molecule-based fluorescent organic nanoassemblies with strong hydrogen bonding networks for fine tuning and monitoring drug delivery in cancer cells. *Small*. 2018;14:1802307. doi:10.1002/smll.201802307
25. Prantner AM, Turini M, Kerfelec B, et al. Anti-mesothelin nanobodies for both conventional and nanoparticle-based biomedical applications. *J Biomed Nanotechnol*. 2015;11:1201–1212. doi:10.1166/jbn.2015.2063
26. Faucon A, Maldiney T, Clément O, et al. Highly cohesive dual nanoassemblies for complementary multiscale bioimaging. *J Mater Chem B*. 2014;2:7747–7755. doi:10.1039/C4TB01199F
27. Hill SA, Benito-Alifonso D, Davis SA, et al. Practical three-minute synthesis of acid-coated fluorescent carbon dots with tuneable core structure. *Sci Rep*. 2018;8:12234. doi:10.1038/s41598-018-29674-2
28. Gueugnon F, Leclercq S, Blanquart C, et al. Identification of novel markers for the diagnosis of malignant pleural mesothelioma. *Am J Pathol*. 2011;178:1033–1042. doi:10.1016/j.ajpath.2010.12.014

29. Quetel L, Meiller C, Assié J-B, et al. Genetic alterations of malignant pleural mesothelioma: association with tumor heterogeneity and overall survival. *Mol Oncol*. 2020;14:1207–1223. doi:10.1002/1878-0261.12651
30. Blondy T, Poly J, Linot C, et al. Impact of RAFT chain transfer agents on the polymeric shell density of magneto-fluorescent nanoparticles and their cellular uptake. *Nanoscale*. 2022;14:5884–5898. doi:10.1039/D1NR06769A
31. Rennick JJ, Johnston APR, Parton RG. Key principles and methods for studying the endocytosis of biological and nanoparticle therapeutics. *Nat Nanotechnol*. 2021;16:266–276. doi:10.1038/s41565-021-00858-8
32. Rodríguez F, Caruana P, De la Fuente N, et al. Nano-based approved pharmaceuticals for cancer treatment: present and future challenges. *Biomolecules*. 2022;12:784. doi:10.3390/biom12060784
33. Pearce AK, O'Reilly RK. Insights into active targeting of nanoparticles in drug delivery: advances in clinical studies and design considerations for cancer nanomedicine. *Bioconjug Chem*. 2019;30:2300–2311. doi:10.1021/acs.bioconjchem.9b00456
34. Attia MF, Anton N, Wallyn J, Omran Z, Vandamme TF. An overview of active and passive targeting strategies to improve the nanocarriers efficiency to tumour sites. *J Pharm Pharmacol*. 2019;71:1185–1198. doi:10.1111/jphp.13098
35. Wicki A, Witzigmann D, Balasubramanian V, Huwyler J. Nanomedicine in cancer therapy: challenges, opportunities, and clinical applications. *J Control Release*. 2015;200:138–157. doi:10.1016/j.jconrel.2014.12.030
36. Saei AA, Yazdani M, Lohse SE, et al. Nanoparticle surface functionality dictates cellular and systemic toxicity. *Chem Mater*. 2017;29:6578–6595. doi:10.1021/acs.chemmater.7b01979
37. Rosenblum D, Joshi N, Tao W, Karp JM, Peer D. Progress and challenges towards targeted delivery of cancer therapeutics. *Nat Commun*. 2018;9:1410. doi:10.1038/s41467-018-03705-y
38. Bahrami B, Hojjat-Farsangi M, Mohammadi H, et al. Nanoparticles and targeted drug delivery in cancer therapy. *Immunol Lett*. 2017;190:64–83. doi:10.1016/j.imlet.2017.07.015
39. Verhaar ER, Woodham AW, Ploegh HL. Nanobodies in cancer. *Semin Immunol*. 2021;52:101425. doi:10.1016/j.smim.2020.101425
40. Bannas P, Hambach J, Koch-Nolte F. Nanobodies and nanobody-based human heavy chain antibodies as antitumor therapeutics. *Front Immunol*. 2017;8:1603. doi:10.3389/fimmu.2017.01603
41. Chanier T, Chames P. Nanobody engineering: toward next generation immunotherapies and immunoimaging of cancer. *Antibodies Basel Switz*. 2019;8:1.
42. Hu Y, Liu C, Muyldermans S. Nanobody-based delivery systems for diagnosis and targeted tumor therapy. *Front Immunol*. 2017;8:1442. doi:10.3389/fimmu.2017.01442
43. Sun S, Ding Z, Yang X, et al. Nanobody: a small antibody with big implications for tumor therapeutic strategy. *Int J Nanomed*. 2021;16:2337–2356. doi:10.2147/IJN.S297631
44. Asaadi Y, Jouneghani FF, Janani S, Rahbarizadeh F. A comprehensive comparison between camelid nanobodies and single chain variable fragments. *Biomark Res*. 2021;9:87. doi:10.1186/s40364-021-00332-6
45. Rossotti MA, Bélanger K, Henry KA, Tanha J. Immunogenicity and humanization of single-domain antibodies. *FEBS J*. 2022;289:4304–4327. doi:10.1111/febs.15809
46. Jovčevska I, Muyldermans S. The therapeutic potential of nanobodies. *Biodrugs*. 2020;34:11–26. doi:10.1007/s40259-019-00392-z
47. Yameen B, Choi WI, Vilos C, et al. Insight into nanoparticle cellular uptake and intracellular targeting. *J Control Release off J Control Release Soc*. 2014;190:485–499. doi:10.1016/j.jconrel.2014.06.038
48. Donahue ND, Acar H, Wilhelm S. Concepts of nanoparticle cellular uptake, intracellular trafficking, and kinetics in nanomedicine. *Adv Drug Deliv Rev*. 2019. doi:10.1016/j.addr.2019.04.008
49. Wang X, Qiu Y, Wang M, et al. Endocytosis and organelle targeting of nanomedicines in cancer therapy. *Int J Nanomed*. 2020;15:9447–9467. doi:10.2147/IJN.S274289
50. Boucard J, Briolay T, Blondy T, et al. Hybrid azo-fluorophore organic nanoparticles as emissive turn-on probes for cellular endocytosis. *ACS Appl Mater Interfaces*. 2019;11:32808–32814. doi:10.1021/acsami.9b12989
51. Bertoglio P, Aprile V, Ambrogi MC, Mussi A, Lucchi M. The role of intracavitary therapies in the treatment of malignant pleural mesothelioma. *J Thorac Dis*. 2018;10:S293–S297. doi:10.21037/jtd.2017.10.165
52. Linot C, Poly J, Boucard J, et al. PEGylated anionic magnetofluorescent nanoassemblies: impact of their interface structure on magnetic resonance imaging contrast and cellular uptake. *ACS Appl Mater Interfaces*. 2017;9:14242–14257. doi:10.1021/acsami.7b01737